Modeling of Double-Angle Shear Connections for Evaluation of Structural Robustness

Judy Liu[1], Joseph Main[2], and Fahim Sadek[3]

[1]Ph.D., Associate Professor, Purdue University, 550 Stadium Mall Drive, West Lafayette, 47907-2051, (765) 494-2254, jliu@purdue.edu
[2]Ph.D., Research Structural Engineer, National Institute of Standards and Technology, 100 Bureau Drive, Stop 8611, Gaithersburg, MD 20899-8611, (301) 975-5286, joseph.main@nist.gov
[3]Ph.D., Leader, Structures Group, National Institute of Standards and Technology, 100 Bureau Drive, Stop 8611, Gaithersburg, MD 20899-8611, (301) 975-4420, fahim.sadek@nist.gov

ABSTRACT

Improved structural robustness is expected for steel gravity load-resisting frames with double-angle shear connections as compared to single-plate connections, given the larger deformation capacity of the double angle. Detailed models of bolted double-angle beam-column connections have been developed for the purpose of evaluating the structural robustness, or resistance to disproportionate collapse, of steel gravity frames. The detailed models have been validated through comparison with available experimental data. Modeling of double-angle connections requires considerations not needed for single-plate connections, such as a reduced ductility in the "k-area" of the angle. Detailed models of two-bay gravity frames were analyzed under "push-down" loading to simulate a column loss scenario. Results for frames with bolted double-angle and single-plate connections show that the larger deformation capacity of the double-angle connection enables larger vertical loads to be sustained with correspondingly larger connection rotations.

INTRODUCTION

While a number of previous studies (e.g., Sadek et al. 2008, Main and Sadek 2012) have investigated the structural robustness of gravity frames with single-plate shear ("shear tab") connections under column loss scenarios, studies of double-angle connection behavior under column loss have been more limited (e.g., Yang and Tan, 2012). The literature on bolted double-angle connections includes experimental and numerical studies on double-angle shear connections, as well as related research on partially restrained top, web, and seat angle connections. The work has largely been focused on creating models for use in analysis of partially restrained frames. While some research has addressed combined shear and tension loading on double-angle shear connections (e.g., Yang et al., 2000), the motivation has been development of component or spring models for capturing moment-rotation response. Such models may not be suited for representing behavior of these connections when subjected to shear and relatively large tensile demands in a column-loss scenario. Under column loss scenarios, double-angle connections offer the potential to sustain larger rotations and axial extensions than shear tab connections through straightening of the angle legs. In this context, determination of the ultimate deformation capacities of the angle legs is critical.

In general, ultimate deformation capacity of angles in connections subjected to tension has not been considered explicitly in prediction equations or numerical models. Some exceptions include work by Shen and Astaneh-Asl (1999, 2000) and Yang and Tan (2012). Yang and Tan (2012) considered a lower ductility near the angle heel, the fracture location, for finite element modeling. Shen and Astaneh-Asl (2000) observed the same failure mode and developed equations for estimating the deformation of the angle at fracture, in addition to predicting stiffness and strength. Shen and Astaneh-Asl's deformation equations did not consider any lower ductility in the heel and were based on an assumption of only tensile strains in the column leg for double-angle connections that did not exhibit prying deformations. Their predictions compared reasonably well to experimental results (within 8 % and 20 %) for their two monotonically loaded bolted angle specimens, both of which fractured near the heel. However, the formulations may result in unconservative predictions for different bolted double-angle configurations.

Yang and Tan (2012) developed numerical models corresponding to 2-D, 2-bay push-down tests of steel frames with different beam-column connections, including a bolted double-angle connection with three bolt rows and 7.9 mm (5/16 in) thick angle. Motivated by studies of Madugula et al., (1997), which showed higher yield stresses in the heel of the angle, Yang and Tan also conducted a pair of tensile coupon tests, using one longitudinal sample taken from an area close to the heel, but still outside of the fillet, or k-area. Tensile coupon test results confirmed higher yield strength in the angle close to the heel, as well as lower ductility. Yang and Tan incorporated these properties into the material models and were able to capture the failure mode observed in the push-down test, which was fracture close to the heel in each angle.

Ductility of k-areas has not been studied for steel angles, but has been for W-shapes, because of the brittle fractures in welded moment connections in the Northridge Earthquake. Tide (2000) conducted tensile tests on longitudinal and transverse k-area coupons from an ASTM A572 Grade 50 W36x150. The k-area percent elongation values at fracture, longitudinal and transverse to the rolling direction, were 15 % and 16.5 %, respectively, for a 25.4 mm (1 in) gage length. Coupons sampled from the web and flange outside of the k-area showed percent elongation greater than 40 % for a 50 mm (2 in) gage length. The yield strength was, on average, about 60 % higher in the k-area than in the web; the tensile strength was about 30 % higher on average. The k-area properties were affected by the rotary straightening process conducted in the mill. Meanwhile, it has been acknowledged that rotary straightening and cold-working of steel angles could also result in lower ductility in the angle k-area, or heel (Rees-Evans, 2011).

In this paper, detailed finite element models capable of capturing the primary mechanisms, deformations and limit states of bolted double-angle connections in tension are described and compared to available experimental data. Modeling of the reduced ductility in the k-area region is necessary in order to capture the failure modes and deformation capacities observed experimentally. The behavior of double-angle connections under column loss is investigated using push-down analysis of a bare (i.e., no slab) two-bay gravity frame with an unsupported center column. Finally, the behavior of shear tab and double-angle connections under column loss is compared.

DETAILED MODELS OF BOLTED DOUBLE-ANGLE CONNECTIONS

This section describes the modeling methodology used for the bolted double-angle connections and presents comparisons with available experimental data. Detailed models of the connections were developed using LS-DYNA, an explicit, general purpose, finite-element software package (Hallquist, 2006). All steel components, including double angles, bolts, and W-shapes, were modeled using fully integrated, 8-node brick elements with selective-reduced integration. Element size for the angles was on the order of 1.3 mm (0.05 in) so as to best capture plastic hinging mechanisms and fracture. Typical element size was about 2.6 mm (0.1 in) in beam and column near connecting elements and about 1.3 mm (0.05 in) in the bolts, following Main and Sadek (2011). Modeling of the heel, or k-area, of the angle, included the radius of the fillet. Components were all initially in contact, with assumed static and dynamic friction coefficients of 0.3.

Inelastic behavior in the steel was represented with a piecewise linear plasticity material model (consisting of seven segments beyond yield), which was calibrated to match data from tensile coupon tests. Beyond the point of necking onset, the strain to failure is dependent upon element size. Therefore, finite element models of tensile coupons with appropriate gage length and element size were used to ensure that calculated engineering stress-strain curves for the models corresponded to the tensile coupon test data. Element erosion, or removal of elements upon reaching an effective plastic strain limit, simulated fracture of the steel. The plastic strain limit for each material was calibrated to match the elongation at fracture from tensile coupon tests. As discussed later, the fracture strain in the k-area of the angle was reduced, compared to the measured percent elongation from tensile coupon tests on samples taken from the angle legs. In the absence of data for the k-area, the stress-strain curve before fracture was unchanged.

Bolt pre-tension, when included, was achieved by including a thermal expansion coefficient in the bolt material model and applying a negative temperature change to the bolt in the initial stages of the analysis. The cross sectional forces in the bolts were monitored to ensure that the desired pre-tension force was achieved. Prescribed motion was applied to the appropriate nodes to load the modeled connections monotonically, simulating a displacement-controlled test of the modeled specimen.

Data from tests by Garlock et al. (2003) were used to confirm that the detailed finite element models could adequately capture the plastic hinging behavior observed in the angles, as well as to evaluate effects of bolt pre-tension, element size and material model. Garlock et al. (2003) conducted cyclic tension tests on bolted top and seat angles and developed methods for modeling the cyclic load-deformation behavior of those angles in analyses of self-centering steel moment resisting frames. Test specimens consisted of two angles back to back, bolted to a W-shape column and a plate simulating a beam flange; a cyclic displacement history was applied at the beam plate. Specimen L6-516-9 was modeled following the detailed approach described above, with symmetry boundary conditions at the simulated beam flange (Figure 1). L6-516-9 was a pair of ASTM A36 L6x6 angles, with 7.9 mm (5/16 in) thickness. A washer plate extending across the angle width was used to create a distinct plastic hinging location in the column leg, which then had an effective gage distance (i.e. corner of heel to inside edge of washer plate) of 95 mm (3.75 in). Tensile test data for tests by Garlock et al. (2003) were provided to the authors. Data for coupons sampled from the angle legs, in the transverse direction, indicated a yield strength of 332 MPa (48 ksi) and a tensile strength of 507 MPa (74 ksi). Fracture strain was 30 % for a gage length of 51 mm (2 in).

Initially, an element size of 2.6 mm (0.1 in) was used for the angles, with no reduction in fracture strain for the k-area, and no bolt pre-tension. Garlock et al. (2003) noted no bolt slip, so bolt holes were modeled with the same diameter as the bolts. Figure 1 shows the experimental results for specimen L6-516-9 compared to the analysis for the first model, with 0 kN pre-tension and a piecewise linear plasticity model (designated MAT024 in LS-DYNA). Angle deformation was measured from the face of the column to the angle heel. The detailed model captures the plastic hinging in the column leg of the angle and resulting softening behavior; the monotonic curve follows the envelope of the cyclic load-deformation, consistent with observations by Shen and Astaneh-Asl (1999).

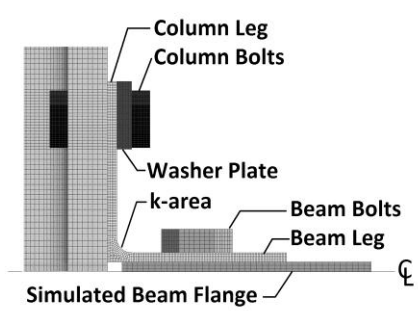

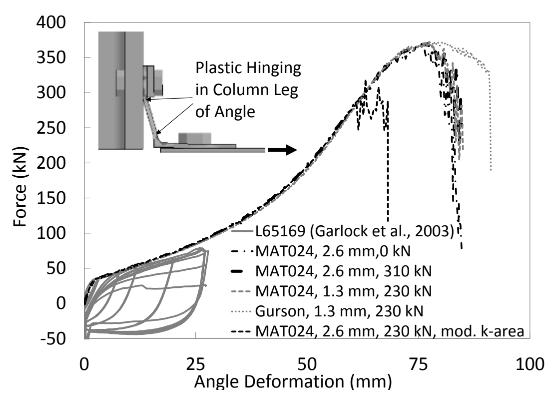

Figure 1: L6-516-9 Detailed Model and Comparison of Analysis to Test Results

Specimen L6-516-9 failed due to low-cycle fatigue at 28 mm (1.1 in), with fracture in the column leg near the heel, or k-area. The detailed model predicted complete tear-out of the column bolt edge distances at about 76 mm (3.0 in). The significant differences between experimental and computational results in both failure mode and deformation were inconsistent with cyclic and monotonic experimental observations by Shen and Astaneh-Asl (1999). Therefore, a number of modeling parameters, including bolt pre-tension, element size, and material model were explored further.

Column bolt pre-tension was investigated to determine if the slip resistance would reduce bolt hole elongation from bolt bearing, mitigating the eventual edge distance tear-out failure. 310 kN (70 kips) of pre-tension was modeled in each bolt, providing more than the minimum specified pre-tension of 230 kN (51 kips) (AISC, 2010) for the 25 mm (1 in) diameter A325 bolts. Regardless, comparison with analysis of the model with the same element size (2.6 mm (0.1 in)) and material model (MAT024, Figure 1) showed no difference in load-deformation or failure mode.

Element size and material model were also investigated. A new L6-516-9 analysis incorporated the Gurson model (e.g., Khandelwal and El-Tawil, 2007), for which ductile fracture is predicted based on void growth, and triaxiality of stresses is considered. Many Gurson parameters used by Khandelwal and El-Tawil (2007) in their study on steel moment frames were adopted; parameters related to fracture were calibrated using analysis of a tensile test coupon with the same element size as the L6-516-9 angle model. Analysis with the Gurson material model, 1.3 mm (0.05 in) elements, and the minimum specified pre-tension of 230 kN (51 kips) in each column bolt again showed little difference compared to a model using the same element size, column bolt pre-tension, and MAT024 (Figure 1). The results also appeared to be insensitive to element size.

Based on the analysis results, MAT024 and 2.6 mm (0.1 in) elements were again adopted. The k-area was modeled with an arbitrary value of half of the effective plastic strain criterion used for the rest of the angle. The value was loosely based on Tide (2000). With the modified k-area, the expected fracture near the heel was obtained at approximately 60 mm (2.4 in) of deformation (Figure 1). Since there were no monotonic tests from Garlock et al. (2003) for comparison of ultimate deformation values, an investigation of modifications to the k-area properties was continued with comparisons to tests by Shen and Astaneh-Asl (1999).

The two bolted double-angle specimens tested monotonically by Shen and Astaneh-Asl (1999) were used for further study of k-area properties. The 10 mm (3/8 in) and 19 mm (3/4 in) thick A36 specimens were identified as Specimen 4 and Specimen 8, respectively. Specimen 4 had a reported yield strength of 338 MPa (49 ksi) and tensile strength of 496 MPa (72 ksi); while specimen 8 had a reported yield strength of 283 MPa (41 ksi) and tensile strength of 434 MPa (63 ksi). Fracture strain was 30 % for both. Specimen 4 was an L4x3.5 with column and beam leg gage distances of 66 mm (2.6 in) and 64 mm (2.5 in). Specimen 8 was an L6x4 with column and beam leg gage distances of 92 mm (3.6 in) and 76 mm (3.0 in). A325 bolts were 19 mm diameter (0.75 in) for Specimen 4 and 25 mm (1.0 in) for Specimen 8, in standard holes of bolt diameter plus 2 mm (0.062 in).

The angles were modeled with 1.3 mm (0.05 in) elements. A parametric study on fixed-ended beams mimicking the deformations and fracture of the angle column leg showed convergence at this element size. Bolts were not pre-tensioned. Shen and Astaneh-Asl (1999) noted effects of bolt slip primarily in the cyclically loaded specimens. Therefore, the bolts were also positioned to be in bearing from the beginning of the monotonic analysis. The piecewise linear plasticity model was calibrated to match stress-strain curves from Shen and Astaneh-Asl (1999). Fracture strain for the k-area was initially the same as in the rest of the angle. Based on the reported 33 mm (1.3 in) deformation at fracture for Specimen 4, and measured strains in the k-area in the detailed model at that level of deformation, a new effective plastic strain criterion was determined. This criterion corresponded to about 18 % engineering strain, or 60 % of the reported elongation.

The new criterion was implemented in the detailed models, which were then able to capture the observed limit state of fracture near the heel for both specimens. Experimental and computational results for Specimens 4 and 8 are compared in Figure 2. Some of the initial prying deformations, observed for Specimen 8 in particular, were not captured by the models, which may partly explain the larger force levels from the computational models., However, predicted ultimate deformation values were at approximately 85% and 93% of the values measured in the experiments for Specimens 4 and 8, respectively, providing further validation of the models.

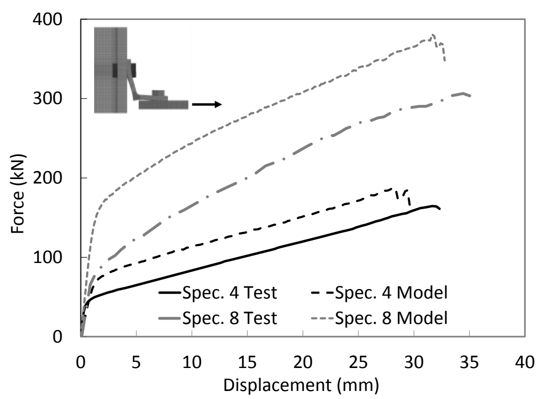

Figure 2: Specimen 4 and 8 Detailed Model Comparisons to Test Results

CONNECTION BEHAVIOR UNDER COLUMN LOSS

The detailed modeling approach, including the modified k-area, was used in a quasi-static simulation of a column loss scenario. The push-down analysis simulated loss of an interior column in a 2-D, 2-bay gravity frame with double-angle connections and 5.5 m (18 ft) spans. The beams and column were A992 W16x26 and W10x49 shapes, respectively. The A572 Grade 50, 216 mm (8.5 in) deep angles were L4x3.5x5/16. Three rows of 19 mm (0.75 in) ASTM F1852N (A325-equivalent, tension control) bolts were placed in standard holes at a column leg gage of 76 mm (3 in) and a beam leg gage of 64 mm (2.5 in). The edge distance for beam web bolt holes was 51 mm (2 in); the top bolt was located at 130 mm (5 in) from the top of beam.

The subassembly was modeled using symmetry boundary conditions and out-of-plane restraint at the column centerline. A pinned support was used at the beam end (Figure 3). A 760 mm (30 in) section of column was modeled with the double-angle connection at mid-height. Solid elements were used for the angles, bolts, column, and a portion of the beam, following the detailed modeling approach, with 1.3 mm (0.05 in) elements for the angles. At 150 mm (6 in) from the beam end, the solid element beam was transitioned to twelve linear beam element segments, each approximately 430 mm (17 in) long. The nodes at the transition from solid elements to beam elements were constrained to move as a rigid body (i.e., compatibility of plane sections).

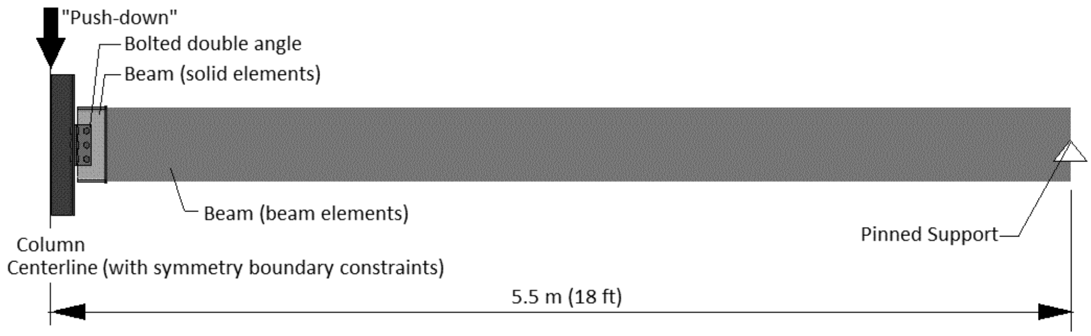

Figure 3: 2-Bay Subassembly Modeled Using Symmetry Boundary Constraints

With minimum specified yield strength of 345 MPa (50 ksi), angle, beam and column steel were assumed to have similar tensile properties as Specimen 4 from Shen and Astaneh-Asl (1999). Specimen 4 material properties, including the same plastic strain criterion for element erosion in the k-area of the angle, were used.

Bolt holes were assumed to be 21 mm (13/16 in) diameter; bolts were centered in the holes. Column bolt pre-tension was not considered, given the analysis results for L6-516-9, and the observations by Shen and Astaneh-Asl (1999). Beam bolt pre-tension and span length were considered as parameters for analysis.

The model with the full, minimum specified bolt pre-tension at the beam bolts was compared to analysis of the same model with no beam bolt pre-tension and half of the full pre-tension. For full pre-tension, beam bolts were tensioned to about 138 kN (31 kip), just above the minimum specified pre-tension of 124 kN (28 kips) (AISC, 2010). The slip resistance caused an initial, compressive force in the beam with vertical displacement of the column. The initial beam axial force versus beam chord rotation response varied with the levels of beam bolt pre-tension, with an initial compressive force response before bolt slip in the connection. The model with full pre-tension exhibited the highest compressive forces; the model with no pre-tension responded only in tension. While there were some differences in the vertical reaction at the beam end, the overall load-deformation response and the chord rotation at fracture were the same.

Results for the original (5.5 m (18 ft)) beam span were compared to analysis of the model with half of that span (2.7 m (9 ft)) and a model with a 9.1 m (30 ft) span (Table 1). Beam bolts were pre-tensioned. Fracture of the double-angle connection occurred at smaller chord rotations for longer spans. Table 1 provides a summary of beam spans and chord rotations corresponding to angle fracture and drop in load. The longest span also showed the highest tension values for the same chord rotations. These observations indicated that, due to geometry of the subassembly, a longer beam span equates with greater elongation at the connection.

Insufficient data was provided in Yang and Tan (2012) for comparison to a detailed model analysis. However, they also tested a 2-bay subassembly with 7.9 mm

(5/16 in) double angles and three bolt rows. As shown in Table 1, results from Yang and Tan (2012) correlate well with the trend of increasing chord rotation to fracture for decreasing span.

Table 1: Beam Span and Ultimate Chord Rotation Values

Beam Span	Chord Rotation (radians)	Source of Value
9.1	0.08	Detailed model (present study)
5.5	0.11	Detailed model (present study)
2.7	0.14	Detailed model (present study)
2.4	0.15	Experiment (Yang and Tan 2012)

COMPARISON OF DOUBLE-ANGLE AND SHEAR TAB CONNECTIONS

Push-down analysis results from the 2-bay subassembly with double-angle connections were compared to previously computed results (Main and Sadek 2012) for a similar subassembly with shear tab connections and beam spans of 6.1 m (20 ft). The slightly longer beam span for the shear-tab subassembly produces a reduction of less than 10 % in rotation for a given column displacement, which is considered sufficiently close to provide a meaningful comparison. Shear tabs had 9.5 mm (3/8 in) A36 plate with three 22 mm (7/8 in) diameter A325 bolts at 76 mm (3 in) spacing, in a single vertical line at 64 mm (2.5 in) from the weld line. The bolt holes were modeled as 1.6 mm (1⁄16 in) larger than the bolt diameter. The beam was an A992 W16x26, and the bolt beam web edge distance was 38 mm (1.5 in). Bolts were not pre-tensioned for the shear tab or double-angle analyses. Details of the shear tab modeling are provided in Main and Sadek (2012).

Based on shear tab and double-angle properties only, the double angle had about 1.6 times the nominal shear strength of the shear tab. However, bolt bearing on the beam web limited the shear capacity of the double-angle connection, resulting in a nominal strength, V_n, which was about 10 % higher than that of the shear tab. Meanwhile, bolt bearing on the beam web limited the nominal tensile capacity, T_n, of the shear tab. Predicted tensile capacities for shear tab and double-angle connections were within 4 %. With similar nominal shear and tensile capacities, the shear tab and double-angle were considered to be comparable connections for the W16x26 beam. A thinner angle would provide the same nominal shear strength in this configuration, and a double-angle with only two bolt rows would not satisfy the connection depth recommended for stability during erection (AISC, 2011).

Figure 4 compares beam axial force, T, and total vertical load, P, at the center column, versus beam chord rotation for the 2-bay subassemblies. Both connections exhibited little to no axial or vertical force initially, due to sliding of the bolts in the holes before coming into bearing. The relative flexibility of the double-angle connection due to deformations and plastic hinging of the angle legs was apparent in the axial and vertical load responses. Drop in capacity began at about 0.06 radians (360 mm (14 in)) of vertical column displacement) due to bolt edge distance tear-out in the beam web for the shear tab connection. A drop occurred at 0.11 radians (580 mm (23 in) of column displacement) due to fracture near the heels of the double angles. While the peak axial force is essentially the same in both cases, the double-angle connection shows greater ductility as well as an ability to support a larger vertical force. However, the drop in resistance is steeper for the angle fracture as compared to the edge distance tear-out.

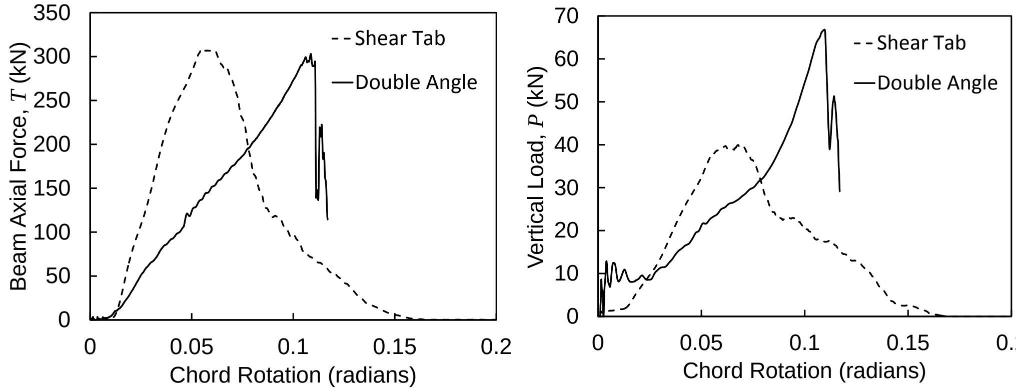

Figure 4: Beam Axial Force, T, and Total Vertical Load, P, versus Chord Rotation for Shear Tab and Double-Angle Subassemblies

CONCLUSIONS

Detailed models of bolted double-angle beam-column connections have been developed and validated using available experimental data. Analysis results demonstrated that a reduction on the order of 40 % for the fracture strain in the k-area was required to capture the failure mode observed in the experiments. The validated models of the connection were used to analyze two-bay gravity frames under "push-down" loading to simulate a column loss scenario. Results for frames with bolted double-angle and shear tab connections were compared. The double angles show greater rotational capacity as well as an ability to support a larger vertical force when compared with the shear tab connection. Future work will consider analyzing a complete composite floor system (e.g., 4 bay x 4 bay), including the floor slab and metal deck to study the contribution of the floor deck to the overall robustness of the gravity framing system.

ACKNOWLEDGMENTS

The authors would like to thank Dr. Maria Garlock, Princeton University, for providing the test and coupon data. This study was partially supported by the NIST/UMD-ARRA Fellowship. Any opinions, findings, conclusions, and recommendations expressed in this paper are those of the writers and do not necessarily reflect the views of the sponsors. Certain commercial software or materials are identified to describe a procedure or concept adequately. Such identification is not intended to imply recommendation, endorsement, or implication by NIST that the software or materials are necessarily the best available for the purpose. The policy of the National Institute of Standards and Technology is to include statements of uncertainty with all NIST measurements. In this document, however, measurements of authors outside NIST are presented, for which uncertainties were not reported and are unknown.

REFERENCES

AISC (2010) "Specification for Structural Steel Buildings," ANSI /AISC 360-10, American Institute of Steel Construction, Chicago, IL.

AISC (2011) "Steel Construction Manual," 14^{th} edition, Chicago, IL, p.10-9.

Garlock, M.M., Ricles, J.M., and Sause, R. (2003). "Cyclic Load Tests and Analysis of Bolted Top-and-Seat Angle Connections," Journal of Structural Engineering, ASCE, 129(12): 1615-1625.

Hallquist, J. (2006). LS-DYNA keyword user's manual, Livermore Software Technology Corporation, Livermore, CA.

Khandelwal, K. and El-Tawil, S. (2007). "Collapse Behavior of Steel Special Moment Resisting Frame Connections." Journal of Structural Engineering, ASCE, 133(5): 646-655.

Madugula, M.K.S., Haidar, R., Monforton, G.R., Marshall, D.G. (1997) "Additional residual stress and yield stress test on hot-rolled angles," Proceedings, Structural Stability Research Council Annual Technical Session, Toronto, Canada; June 1997. p. 55–68.

Main, J.A. and Sadek, F. (2011). "Modeling of bolted connections for collapse analysis of steel structures." Proceedings, 14th International Symposium on Interaction of the Effects of Munitions with Structures, Seattle, Washington, September 19-23, 2011.

Main, J.A. and Sadek, F. (2012). "Collapse Resistance of Steel Gravity Frame Systems: Computational Assessemnt." *NIST Technical Note*, National Institute of Standards and Technology, Gaithersburg, MD.

Rees-Evans, D. (2011). "Re: Steel Angle Question," message to first author, 27 Sept. 2011, e-mail.

Sadek, F., El-Tawil, S., and Lew, H.S. (2008). "Robustness of composite floor systems with shear connections: modeling, simulation, and evaluation." Journal of Structural Engineering, ASCE, 134(11), 1717-1725.

Shen, J. and Astaneh-Asl, A. (1999) "Hysteretic behavior of bolted-angle connections," Journal of Constructional Steel Research, Vol. 51, pp. 201–218.

Shen, J. and Astaneh-Asl, A. (2000) "Hysteresis model of bolted-angle connections," Journal of Constructional Steel Research, Vol. 54, pp. 317–343.

Tide, R.H.R. (2000) "Evaluation of steel properties and cracking in "k"-area of W shapes," Engineering Structures, Vol. 22, Issue 2, pp. 128-134.

Yang, B. and Tan, K.H. (2012) "Numerical analyses of steel beam–column joints subjected to catenary action," Journal of Constructional Steel Research, Vol. 70, pp. 1–11.

Yang, J.-G., Murray, T.M., Plaut, R.H. (2000) "Three-dimensional finite element analysis of double-angle connections under tension and shear," Journal of Constructional Steel Research, Vol. 54, Issue 2, pp. 227–244.